

Recognition of T-rich single-stranded DNA by the cold shock protein *Bs*-CspB in solution

Markus Zeeb, Klaas E.A. Max¹, Ulrich Weininger, Christian Löw, Heinrich Sticht² and Jochen Balbach*

Laboratorium für Biochemie, Universität Bayreuth, D-95440 Bayreuth, Germany, ¹Max-Delbrück-Centrum für Molekulare Medizin, 13125 Berlin, Germany and ²Institut für Biochemie, Emil-Fischer-Zentrum, Universität Erlangen–Nürnberg, 91054 Erlangen, Germany

Received December 6, 2005; Revised February 28, 2006; Accepted April 30, 2006

ABSTRACT

Cold shock proteins (CSP) belong to the family of single-stranded nucleic acid binding proteins with OB-fold. CSP are believed to function as 'RNA chaperones' and during anti-termination. We determined the solution structure of *Bs*-CspB bound to the single-stranded DNA (ssDNA) fragment heptathymidine (dT₇) by NMR spectroscopy. *Bs*-CspB reveals an almost invariant conformation when bound to dT₇ with only minor reorientations in loop β1–β2 and β3–β4 and of few aromatic side chains involved in base stacking. Binding studies of protein variants and mutated ssDNA demonstrated that *Bs*-CspB associates with ssDNA at almost diffusion controlled rates and low sequence specificity consistent with its biological function. A variation of the ssDNA affinity is accomplished solely by changes of the dissociation rate. ¹⁵N NMR relaxation and H/D exchange experiments revealed that binding of dT₇ increases the stability of *Bs*-CspB and reduces the sub-nanosecond dynamics of the entire protein and especially of loop β3–β4.

INTRODUCTION

A rapid reduction in growth temperature induces the cold shock response of many prokaryotic organisms by down-regulation of the expression of most proteins (1) and transient up-regulation of a small set of proteins (2,3). These induced proteins include the transcription factor NusA, initiation factor IF2, ribosomal proteins L7/L12 and S6, ribosome-binding factor RbfA, prolyl isomerase PPIB (4) and, most prominently, the family of cold shock proteins, CSP (1). CSP

stimulate the transcription of cold shock inducible genes (5) and the initiation of translation by destabilizing non-productive secondary structures in mRNA at low temperature (6). Therefore, CSP are denoted as RNA chaperones, because binding of mRNA is sequence unspecific (7–9). Destabilizing of secondary structures of single-stranded nucleic acids takes place in anti-termination, which leads to the induction of various cold shock genes at low temperature (4,10–12). In cell-free transcription and translation, however, CSPs block the bulk protein expression (13). The 5'-untranslated regions (5'UTRs) of *Csp* mRNAs contain high affinity binding sites for ribosomes, which are responsible for a very effective initiation of CSP translation (14,15). This redistribution of the ribosomes might block the translation of other proteins at low temperature (16).

In *Bacillus subtilis*, three CSP (*Bs*-CspB, *Bs*-CspC and *Bs*-CspD) have been identified, which can complement each other *in vivo*, but a knock out of all three CSP genes is lethal (17). The structure of the 67 amino acid encompassing protein *Bs*-CspB revealed a β-barrel with an OB-fold (18) formed by five antiparallel β-strands (19,20). The structure of the CSP is conserved in mesophilic, thermophilic and hyperthermophilic bacteria, such as *Ec*-CspA from *Escherichia coli* (21–23), *Bc*-Csp from *Bacillus caldolyticus* (24) and *Tm*-Csp from *Thermotoga maritima* (25). One unique feature of their structures is the numerous solvent exposed aromatic side chains (W8, F9, F15, F17, H29, F30, F38 in *Bs*-CspB) from which F15, F17, F27 and H29 significantly increase the thermodynamic stability of the protein (26,27). They are part of the nucleic acid-binding motifs RNP1 and RNP2, which have been identified by sequence alignment (28,29). Our detailed structural knowledge of OB-folded nucleoprotein complexes in solution is restricted to telomere DNA-binding proteins (30–32).

In the present paper we determined the conformation of *Bs*-CspB bound to the single-stranded DNA (ssDNA) fragment dT₇ by NMR spectroscopy in solution. The structural

*To whom correspondence should be addressed. Tel: +49 345 55 25353; Fax: +49 345 55 27383; Email: jochen.balbach@physik.uni-halle.de
Present addresses:

Markus Zeeb, Department of Molecular Biology, The Scripps Research Institute, La Jolla, USA

Ulrich Weininger, Christian Löw and Jochen Balbach, Fachbereich Physik, Fachgruppe Biophysik, Martin-Luther-Universität Halle-Wittenberg, D-06099 Halle(Saale), Germany

© 2006 The Author(s).

This is an Open Access article distributed under the terms of the Creative Commons Attribution Non-Commercial License (<http://creativecommons.org/licenses/by-nc/2.0/uk/>) which permits unrestricted non-commercial use, distribution, and reproduction in any medium, provided the original work is properly cited.

analysis of the *Bs*-CspB/dT₇ complex dominated by hydrophobic interactions between aromatic protein side chains and ssDNA bases is accompanied by a mutational analysis of the thermodynamics and kinetics of the complex formation by equilibrium and stopped-flow fluorescence spectroscopy. High affinity binding with nanomolar dissociation constants correlates with a low dissociation rate and an invariant, almost diffusion controlled association rate for wild-type *Bs*-CspB when compared with numerous protein variants. H/D exchange experiments and ¹⁵N NMR relaxation of free and ssDNA-bound *Bs*-CspB revealed the changes in stability and dynamics of the *Bs*-CspB/dT₇ complex when compared to free *Bs*-CspB.

MATERIALS AND METHODS

Wild-type *Bs*-CspB from *B. subtilis* and its variants were expressed and purified as described previously (33) with minor modifications. Deoxyoligonucleotide dT₇ and other ssDNA fragments were purchased from MWG Biotech AG (Germany). *Bs*-CspB and dT₇ concentrations were determined by the absorbance at 280 and 260 nm using extinction coefficients of 5800 M⁻¹ cm⁻¹ (27) and 58 800 M⁻¹ cm⁻¹, respectively. The extinction coefficients of various ssDNA sequences were calculated as sum of the extinction coefficient of the individual nucleotides.

NMR measurements

NMR spectra for structure determination were acquired at 15°C on Bruker DRX500, Avance 600, DMX750 and Avance 900 spectrometers in 50 mM Na-cacodylate, 3 mM MgCl₂, pH 7.0. NMR spectra for the relaxation study were recorded at 25°C in 100 mM Na-cacodylate, pH 7.0. External referencing of proton chemical shifts was achieved by using 2,2-dimethyl-2-silapentane-5-sulfonate (DSS).

Formation of the *Bs*-CspB/dT₇ complex was accomplished by titration of 0.8 mM uniformly labeled ¹⁵N *Bs*-CspB with unlabeled dT₇ at 500 MHz. Most of the backbone amides experience fast exchange with respect to the NMR chemical shift timescale and therefore could be directly assigned by tracking the gradually shifting crosspeaks starting from the unbound protein. The mean weighted change (34) in chemical shifts between apo and holo *Bs*-CspB of the backbone resonances were calculated according to $\Delta(\delta_{MW}^{1H, 15N}) = (((\delta^{1H})^2 + 1/25(\delta^{15N})^2)/2)^{0.5}$ and $\Delta(\delta_{MW}^{1H\alpha, 13C\alpha}) = (((\delta^{1H\alpha})^2 + 1/10(\delta^{13C\alpha})^2)/2)^{0.5}$. Assignment of crosspeaks in the slow chemical exchange regime was carried out with standard 3D ¹⁵N-edited NOESY- and TOCSY-HSQC spectra at 500 MHz. Standard triple resonance experiments [HNCACB (35), CBCA(CO)NH (36) and HNCO (37)] for the backbone assignments were recorded on a ¹³C,¹⁵N-labeled sample of *Bs*-CspB in complex with unlabeled dT₇ at 600 MHz in 93% H₂O/7% D₂O. Aliphatic side chain assignment was performed using H(C)(CO)NH- and C(CO)NH-TOCSY experiments (37) in H₂O as well as HCCH-COSY experiments in D₂O (38). Additionally, aromatic side chains were assigned from (H β)C β (C γ C δ)H δ and (H β)C β (C γ C δ C ϵ)H ϵ spectra (39).

A 2D ¹⁵N-edited NOESY at 750 MHz and a 3D ¹⁵N-edited NOESY-HSQC (40) at 500 MHz with mixing times of

150 ms were recorded with a sample containing ¹⁵N-labeled *Bs*-CspB and unlabeled dT₇. ¹H homonuclear 2D NOESY spectra in D₂O with mixing times between 80 and 150 ms were acquired at 500 MHz on a fully unlabeled sample. Additionally, 3D ¹³C-edited HMQC-NOESY spectra were recorded in D₂O with altered ¹³C carrier frequencies to observe aliphatic or aromatic carbons, respectively. Attempts to assign resonances and intramolecular NOEs of the dT₇ oligonucleotide with 2D double-half-filtered NOESY (mixing times between 100 and 250 ms) and 2D double-half-filtered TOCSY spectra at 600 and 900 MHz (41,42) or 2D ¹³C/¹⁵N F₁-filtered NOESY experiments (43) at 600 MHz were unsuccessful. Intermolecular NOEs between *Bs*-CspB and dT₇ were determined by 2D ¹³C F₁-edited, F₂-filtered NOESY spectra (42) but remained also unassigned. NOEs identified in the double-half-filtered (intramolecular NOEs of dT₇) and filtered-edited (intermolecular NOEs) spectra assisted in identification of these crosspeaks in the homonuclear and ¹⁵N or ¹³C-edited NOESY experiments from which distance restraints for the structure calculation were derived. Subsequently, these NOEs were omitted from the latter. Additionally, coupling constants were obtained from an HNHA experiment (44) and residual dipolar couplings (RDCs) were determined in a weakly oriented sample of ¹⁵N *Bs*-CspB in 18 mg/ml filamentous phage Pf1 (Asla). HN-N RDCs were measured from IPAP-[¹H-¹⁵N]-HSQC experiments (45). For the comparison of translational diffusion of *Bs*-CspB and *Bs*-CspB/dT₇, a PFG-SLED pulse sequence (46) was employed.

Potential hydrogen bond donors were identified from H/D exchange experiments by dissolving lyophilized ¹⁵N *Bs*-CspB/dT₇ complex in D₂O and subsequent collection of a series of 2D ¹⁵N HSQC spectra. Protection factors (*P*) were derived from $P = k_{int}/k_{ex}$, where *k*_{int} is the intrinsic exchange rate constant and *k*_{ex} is the observed exchange rate constant of a backbone amide. *k*_{int} was calculated on the basis of model peptides (47) and *k*_{ex} was obtained by fitting a single exponential function without offset to the intensity decay of crosspeaks in the recorded 2D HSQC spectra.

For the ¹⁵N relaxation study of free and dT₇ bound *Bs*-CspB NMR spectra for the determination of *R*₁, *R*₂ and heteronuclear NOE (hNOE) were recorded at a Bruker DRX500 at 25°C as described recently (48). Model-free analyses and iterative optimization of Lipari-Szabo motional parameters were performed with the program MODELFREE (49) (version 3.1) as described by using an isotropic tumbling model (48).

Structure calculation and analysis

NOE crosspeaks were manually classified as strong, medium or weak according to their intensities and converted into distance restraints of <3.0, 4.0 or 5.5 Å, respectively. Scalar ³J_{HN,H α} coupling constants of either <6.0 Hz or >8.0 Hz were restrained to adopt phi torsion angles between -80° and -40° or between -160° and -80°, respectively (45,50). Slow exchanging hydrogens were identified from amide proton exchange experiments. For each of the assigned 23 hydrogen bonds the distance between the amide proton and the acceptor was restrained to <2.3 Å and the distance between the amide nitrogen and the acceptor to <3.3 Å.

This structural information served as an input for the calculation of 120 structures using restrained molecular dynamics with XPLOR-NIH-1.2.1 (51). A three-stage simulated annealing protocol (52) with floating assignment of prochiral groups (53) was carried out using the following simulation procedure. For conformational space sampling 60 ps with a time step of 3 fs were simulated at a temperature of 2000 K, followed by 80 ps of slow cooling to 1000 K, and 50 ps of cooling to 100 K, both with a time step of 2 fs. A conformational database term for both backbone and side chain dihedral angles (54) with the described modification (55) was included in the target function in order to improve the stereochemical properties of the structures. After simulated annealing the structures were subjected to 1000 steps of energy minimization, the final 500 steps without conformational database potential. The 60 lowest energy structures were subject to refinement with HN-N RDCs as described previously (56) and the 18 lowest energy structures having no NOE distance restraint violations >0.15 Å and no ϕ -angle restraint violations $>0.5^\circ$ were selected for further characterization. The geometry of the structures, structural parameters and elements of secondary structure were analyzed using the programs DSSP (57) and PROCHECK (58,59) revealing 89.8% of the residues in the core region of the Ramachandran plot, 9.7% in the additionally allowed regions and 0.5% in the generously allowed regions. The molecular structure figures were generated using MolMol (60) and PyMOL [DeLano, W. (2003), <http://www.pymol.org>]. This family of 18 structures has been deposited in the Protein Data Bank under the accession code 2F52.pdb (RCSB035462).

Fluorescence quenching

The intrinsic fluorescence of *Bs*-CspB Trp8 is quenched upon binding to nucleic acids and therefore was used as a sensitive probe to monitor binding in equilibrium and kinetic experiments. Binding affinities were determined by equilibrium titration experiments as described previously (27) whereby

protein concentrations of 25, 100 or 200 nM were used depending on dissociation constants (K_D) of the respective protein variant to dT₇ or of wild-type *Bs*-CspB to the various ssDNA fragments. To obtain the stoichiometry of the respective nucleoprotein complexes protein concentrations between 2 and 10 μ M were used.

Association kinetics were monitored by quenching of the intrinsic tryptophan fluorescence of *Bs*-CspB by the ssDNA fragments in a sequential stopped-flow mixing device and analyzed as described elsewhere (27). Protein concentrations of 30 or 300 nM were used depending on the K_D of the respective *Bs*-CspB variant and dT₇ end concentrations up to 1.2 μ M were employed.

RESULTS

NMR titration of *Bs*-CspB by heptathymidine dT₇

Various affinities and stoichiometries have been reported for different nucleoprotein complexes with *Bs*-CspB (7–9,27). Therefore, a systematic search for a high affinity ssDNA fragment was performed (Table 1) including potential physiological target sequences (Y-box and cold box fragments). The heptathymidine fragment dT₇ revealed the lowest K_D of 1.8 nM at a 1:1 stoichiometry and was therefore selected for further investigations. An NMR titration of ¹⁵N enriched *Bs*-CspB sample with unlabeled dT₇ was performed and a superposition of the first and last HSQC spectrum is depicted in Figure 1. Most amide protons showed fast exchange on the NMR chemical shift time scale allowing a direct assignment of the amide resonances in the *Bs*-CspB/dT₇ complex from the gradual shift during the titration. The following residues stand out from the mean weighted change in chemical shifts $\Delta(\delta_{MW}(^1\text{H}, ^{15}\text{N}))$ and $\Delta(\delta_{MW}(^1\text{H}^\alpha, ^{13}\text{C}^\alpha))$ of the backbone resonances (34) between apo and holo *Bs*-CspB: β -strand 1 (K7, W8 side chain, N10), β 1– β 2 loop (S11, E12), RNP1 motif (K13, G14, F15, F17, G16, V20), β -strand 3 (D25), RNP2 motif (V26, F27, V28, H29, F30), β 3– β 4 loop (S31, I33,

Table 1. Dissociation constants and stoichiometries of *Bs*-CspB/ssDNA complexes from tryptophan fluorescence titration experiments^a

Fragment	Number of nucleotides (%T)	ssDNA sequence	<i>Bs</i> -CspB:ssDNA	K_D (nM)
dT ₄	4 (100)	TTT T	1:1	3205 \pm 150
dT ₅	5 (100)	TTT TT	1:1	940 \pm 10
dT ₆	6 (100)	TTT TTT	1:1	326 \pm 20
dC ₆	6 (0)	CCC CCC	1:1	12600 \pm 1000
dT ₇	7 (100)	TTT TTT T	1:1	1.8 \pm 0.4
Y-box5 ^b	5 (40)	ATT GG	1:1	5300 \pm 1000
Y-box7 ^b	7 (57)	TAT TGG T	1.4:1	530 \pm 50
Y-box12 ^b	12 (25)	CTG ATT GGC CAA	1.9:1	2030 \pm 390
Y-box25 ^b	25 (28)	ATC CTA CTG ATT GGC CCA GGT GCT G	3:1	3920 \pm 45
dcbl ^c	7 (57)	TTA TTA G	1:1	20 \pm 3
dcbl _a ^c	13 (69)	ATT ATT TTT GTT C	2:1	44 \pm 2
dcbl _b ^c	13 (8)	GAG CAA GAA TAG G	2:1	1160 \pm 90
dcbl _{br} ^c	13 (8)	GGA TAA GAA CGA G	2:1	1090 \pm 110
dcbl _a ^c	17 (41)	TTT AAG AAG AAA GTT TT	2:1	460 \pm 34
dcbl _b ^c	16 (43)	GAG TTT TGG TCT TGA A	2:1	43 \pm 2
dcbl _{br} ^c	16 (43)	AAG TTC TGG TTT TGA G	2:1	30 \pm 2
dcbl _{ds} ₁₃ ^c	13 (46)	GTT TTG TAA GAG T	2:1	66 \pm 21

^aAll experiments were performed at 15°C in 50 mM Na-cacodylate, pH 7.0, and 100 mM KCl.

^bssDNA fragments containing the Y-box motif ATTGG (underline).

^cssDNA fragments deduced from the 5'-UTR of *Bs*-CspB mRNA.

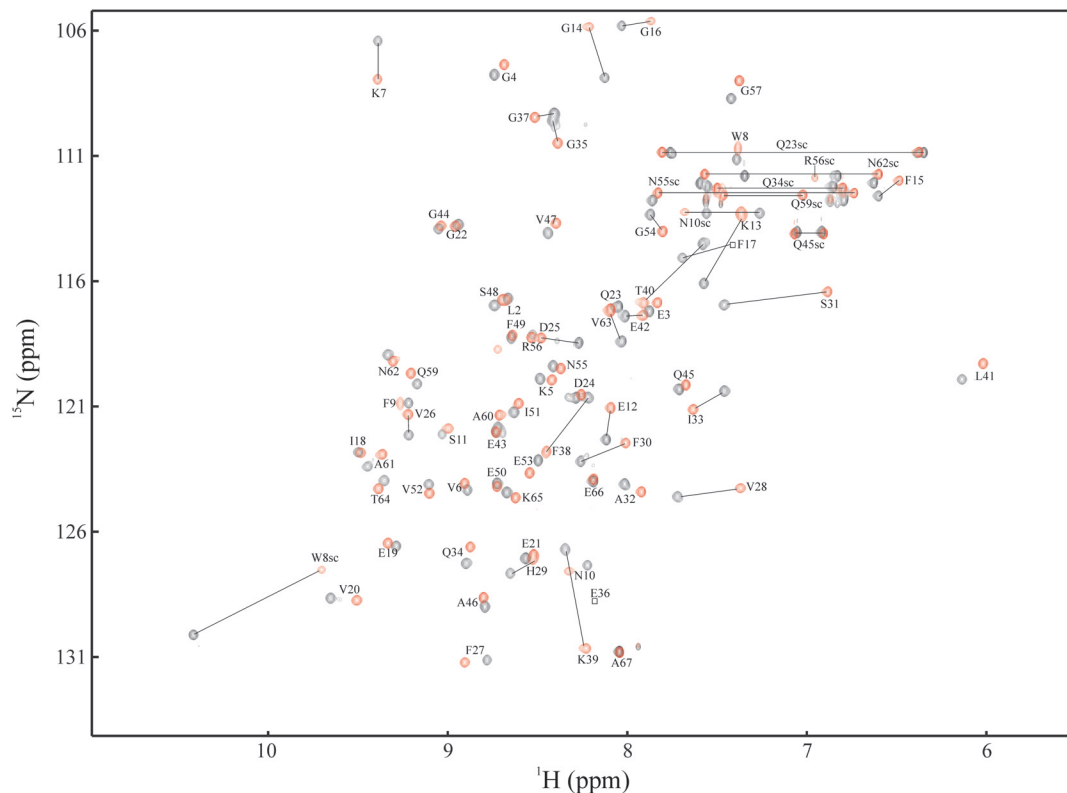


Figure 1. The 2D $^1\text{H}/^{15}\text{N}$ HSQC spectrum of free (black) and dT₇-bound (red) *Bs*-CspB in 50 mM Na-cacodylate, 3 mM MgCl₂, pH 7.0 at 15°C. The spectra were recorded at a *Bs*-CspB-concentration of 0.8 mM and a final dT₇ concentration of 1.2 mM.

G35, F38, K39, T40, L41, E42), β -strand 4 (G54), β 4- β 5 loop (R56), and β -strand 5 (G57, P58, Q59 backbone and side chain). These residues of *Bs*-CspB facilitate the binding of dT₇ either by direct interaction or by conformational rearrangements remote from the binding interface. Significant $\Delta(\delta(^1\text{H}))$ values for the H^B protons include F15, D25, F30, Q34 and N62.

Structure determination of the protein conformation of *Bs*-CspB in complex with dT₇

The experimental constraints, which were employed for the structure calculations of *Bs*-CspB in complex with dT₇ are summarized in Table 2. Possible backbone hydrogen bond donors have been determined from the protection factors (47) derived by H/D exchange experiments (Figure 2). Several NMR experiments were performed to assign the dT₇ resonances in the complexed form and to identify intermolecular NOE effects between *Bs*-CspB and the oligonucleotide dT₇, including 2D $^{13}\text{C}(\omega_1, \omega_2)$ double half-filtered NOESY and 2D $^{13}\text{C}/^{15}\text{N}(\omega_1)$ -filtered NOESY experiments of $^{13}\text{C}/^{15}\text{N}$ *Bs*-CspB in complex with unlabeled dT₇. Additionally, homonuclear or ^{15}N -edited ^1H NOESY spectra of partially deuterated ^{15}N -labeled *Bs*-CspB in complex with protonated dT₇ were analyzed. Owing to the lack of dispersion of the homonucleotide sequence of dT₇, an unambiguous assignment of the resonances of either uncomplexed or complexed dT₇ was not successful. Therefore, the conformation of dT₇ in complex with *Bs*-CspB could not be determined by NMR spectroscopy.

An overlay of the protein backbone of the 18 lowest energy structures of the *Bs*-CspB conformation in complex with dT₇ is given in Figure 3 and compared with the NMR structure of apo *Bs*-CspB (19). The conformation of the five strands of the β -barrel reveals only small differences and serves as a pre-formed scaffold for ssDNA recognition. Backbone deviations of the two NMR families of structures occur in loop β 1- β 2 and loop β 3- β 4. The latter loop remains less well defined with bias in its orientation towards loop β 1- β 2. We are to some extent limited in the analysis of the side chain conformations of those aromatic residues, which are involved in stacking interactions with dT₇ (see below), because the conformation of the nucleic acid could not be calculated and the missing intermolecular NOEs cause overvaluing of the intramolecular NOEs. Additionally, a comparison of the side chain conformations of F15, F27, F29 and F38 is not straightforward because they are not very well defined in the solution structure of free *Bs*-CspB (19). Beside those, W8 is well defined in both the free and dT₇ bound form and shows an almost perpendicular orientation. This is consistent with the strong quench of the tryptophan fluorescence observed upon ssDNA binding (see below).

Mutational analysis of the thermodynamics and kinetics of *Bs*-CspB/dT₇

Based on the above-described structural elucidations, a set of protein variants has been selected to verify the role of the respective residue in dT₇ binding by equilibrium and time resolved fluorescence spectroscopy. In the *Bs*-CspB/dT₇

Table 2. Experimental restraints and structural statistics (for the calculation of the tertiary structure of *Bs*-CspB in complex with the ssDNA fragment dT₇)

Number of experimental restraints				
Distance restraints from NOEs				
Interresidual NOEs	Sequential	($ i - j = 1$)	283	
	Medium long range	($ i - j < 5$)	135	
	Long range	($ i - j \geq 5$)	411	
Intraresidual NOEs				
Dihedral angle restraints ϕ/χ_1			381	
RDC restraints (D_{N-HN})			29/2	
Hydrogen bond restraints			50	
			23	
Molecular dynamics statistics				
Average energy (kcal/mol)	E_{tot}	31.0 ± 3.0		
	E_{bond}	0.9 ± 0.1		
	E_{angle}	10.2 ± 1.2		
	$E_{improper}$	2.7 ± 0.6		
	E_{vdw}	7.6 ± 1.5		
	E_{NOE}	3.3 ± 1.2		
	E_{cdih}	0.1 ± 0.02		
	E_{RDC}	6.1 ± 1.1		
r.m.s.d. from ideal distance (Å)	Bonds	0.00096 ± 0.00007		
	NOE	0.012 ± 0.001		
r.m.s.d. from ideal angles (degree)	Bond angles	0.190 ± 0.012		
	Improper angles	0.287 ± 0.016		
r.m.s.d. from dipolar couplings (Hz)	HN-N couplings	0.071 ± 0.014		
Atomic r.m.s.d. (Å) of 18 refined <i>Bs</i> -CspB structures ^a				
All residues ^b	0.54 (backbone)	0.94 (heavy atoms)		
Secondary structure ^c	0.21 (backbone)	0.55 (heavy atoms)		
Pairwise backbone r.m.s.d. (Å) between different <i>Bs</i> -CspB structures				
	NMR(bound) ^d	X-ray(bound) ^e	X-ray(free) ^f	NMR(free) ^g
NMR(bound)	0	1.44^h (0.87) ^c	1.34 (0.80)	1.68 (1.08)
X-ray (bound)	—	0	0.92 (0.37)	1.90 (1.37)
X-ray(free)	—	—	0	1.66 (1.28)
NMR(free)	—	—	—	0

^aThe final force constants used in the structure calculation were $1000 \text{ kcal}\cdot\text{mol}^{-1}\cdot\text{Å}^{-2}$ for the bond length, $500 \text{ kcal}\cdot\text{mol}^{-1}\cdot\text{rad}^{-2}$ for the bond angles and improper angles, $50 \text{ kcal}\cdot\text{mol}^{-1}\cdot\text{Å}^{-2}$ for the NOE distance restraints, $55 \text{ kcal}\cdot\text{mol}^{-1}\cdot\text{rad}^{-2}$ for the ϕ -angle restraints, and $1.0 \text{ kcal}\cdot\text{mol}^{-1}\cdot\text{Hz}^{-2}$ for the RDCs.

^bCalculated for the final set of 18 structures (residue 1–67).

^cCalculated for the elements of regular secondary structure (residues 2–10, 15–19, 26–32, 46–53, 59–65).

^dAverage structure from this study.

^eCrystal structure of ssDNA-bound *Bs*-CspB (2ES2.pdb).

^fCrystal structure of the free *Bs*-CspB (1CSP.pdb) (20).

^gNMR average structure of the free *Bs*-CspB(1NMG.pdb) (19).

^hCalculated for residues 1–67.

complex, the intrinsic fluorescence of W8 is 80% quenched compared to the apo protein. This sensitive probe allows the determination of dissociation constants (K_D) as well as association (k_{on}) and dissociation (k_{off}) rate constants of the wild-type nucleoprotein and its variants. A stoichiometric titration of *Bs*-CspB monitored by fluorescence quenching and the analysis of NMR chemical shifts of backbone resonances as described elsewhere (27) revealed a 1:1 stoichiometry for *Bs*-CspB/dT₇ within a concentration range of nano- to millimolar (data not shown). Table 3 shows a summary of K_D , k_{on} and k_{off} values of *Bs*-CspB/dT₇ and 18 nucleoprotein variants derived from fluorescence experiments.

The dissociation constants show that aromatic residues at positions 15, 17, 27, 29, 30 and 38 are essential for a tight binding of dT₇. Substitutions with non-aromatic residues at these positions result in an at least 50-fold increase of K_D , whereas substitutions by aromatic residues (position 15 and 30) lead to wild-type affinities towards dT₇. The latter two substitutions are based on a sequence alignment of *Bs*-CspB with *Bc*-Csp and *Tm*-Csp (27). A change in the electrostatics and polarity at positions K7, K13, D25, R56 and Q59 lead to less pronounced changes in the nucleotide binding affinity. The conformational freedom allowed by glycine at positions

35 and 54 is not required for a tight binding as tested by the alanine variants. A strong reduction of possible backbone Φ angles at these positions by substitution with proline, however, increased K_D significantly. G35 and G54 are part of the loops $\beta 3$ – $\beta 4$ and $\beta 4$ – $\beta 5$, respectively, confining the binding surface of *Bs*-CspB, and for which sufficient conformational freedom is required for tight binding. The P58A variant remains silent in this respect.

The dissociation constant at equilibrium reflects the ratio between the k_{on} and k_{off} rate constants of complex formation. To gain deeper insights, both rates have been determined experimentally by rapid mixing of the protein solutions with various amounts of oligonucleotides in a stopped-flow fluorescence spectrometer. Under pseudo first-order conditions (27), k_{on} is the slope of the ssDNA concentration dependence of $k_{obs} = k_{on} \cdot [\text{ssDNA}] + k_{off}$ and therefore better determined than the offset k_{off} , which results from an extrapolation to 0 M ssDNA. Therefore, k_{off} is often determined by $k_{off} = k_{on} \cdot K_D$. These values are also given in Table 3. All k_{on} and k_{off} rate constants of the protein variants have in common that k_{on} is almost invariant whereas k_{off} varies up to a factor of 100 according to the respective K_D . Consequently, the reduced affinity of mutated *Bs*-CspB towards

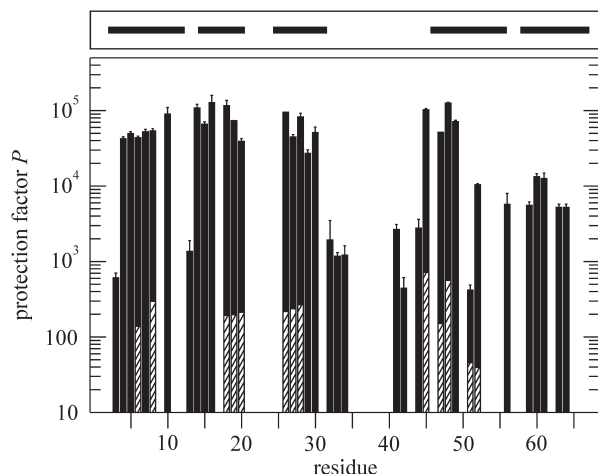


Figure 2. Protection factors of amide protons from H/D exchange of free (hatched bars) and dT₇-bound (solid bars) *Bs-CspB*. Missing bars indicate amides, which got fully deuterated in the dead-time of the experiment (5 min). The solid bars on top represent the five β -strands of *Bs-CspB*.

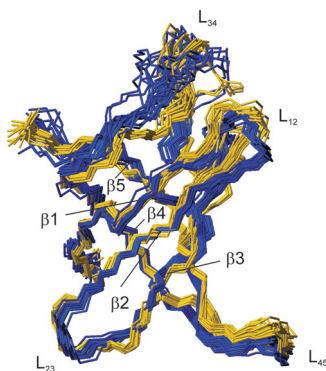


Figure 3. Backbone superposition of the 18 lowest energy NMR structures of free [blue, 1NMF.pdb (19)] and dT₇-bound (yellow) *Bs-CspB*. The five β -strands and their connecting loops are indicated. The r.m.s.d. values of dT₇-bound *Bs-CspB* of all 67 residues are 0.54 Å (backbone) and 0.94 Å (all heavy atoms). Main deviations between apo and holo form of *Bs-CspB* are located in loop β 1– β 2 (L₁₂) and loop β 3– β 4 (L₃₄).

dT₇ results from an increased dissociation rate. A set of experiments, where binding kinetics were determined for wild-type *Bs-CspB* and cytosine doped T-rich ssDNA fragments (bottom of Table 3), leads to the same conclusion.

¹⁵N NMR relaxation study of the dynamics of *Bs-CspB*/dT₇

Complex formation e.g. in the framework of an induced fit model should be reflected in a change of the protein dynamics. Therefore, the dynamics of *Bs-CspB*/dT₇ were determined by an extended Lipari-Szabo analysis of ¹⁵N relaxation rates and hNOE effects. Figure 4 depicts a comparison of hNOE, general order parameter S^2 , and chemical exchange contributions (R_{ex}) to R_2 of *Bs-CspB*/dT₇ with free *Bs-CspB*. hNOE and S^2 reflect large amplitude motions of each backbone N-H vector on a nanosecond-to-picosecond timescale and R_{ex} on a millisecond-to-microsecond timescale. The overall rotational correlation time for *Bs-CspB* and

Bs-CspB/dT₇ was very similar (4.4 and 4.0 ns, respectively). Consequently, the observed 1:1 stoichiometry of the *Bs-CspB*/dT₇ complex in solution is realized by protein and ssDNA monomers. The vast majority of backbone amides show increased hNOE and S^2 values upon dT₇ binding. All residues in the five β -strands show this trend indicating a loss of internal flexibility of the entire protein chain in *Bs-CspB*/dT₇. F30 is the only backbone amide, which has a strongly decreased S^2 value in the complex (0.65) compared with *Bs-CspB* (0.85). In contrast, S^2 values of the N-terminus of loop β 3– β 4 (F38–E43) increase upon binding to values of the adjacent β -strands. This indicates a loss in dynamics and explains the better-defined NMR structure of this region compared to the free form (Figure 3). The order parameters of all other aromatic residues involved in binding show high values in both the free and complexed form of *Bs-CspB*.

The R_{ex} chemical exchange contributions to R_2 show remarkable differences for free *Bs-CspB* and *Bs-CspB*/dT₇. In the free form of *Bs-CspB*, all backbone amides reveal R_{ex} contributions from global unfolding and refolding of the protein even under native buffer conditions (refolding rate constant $k_f = 1070 \text{ s}^{-1}$ and the unfolding rate constant $k_u = 12 \text{ s}^{-1}$) (33,48,61,62). Upon binding, all R_{ex} rate constants beside W8 drop below 2 Hz indicating that the addition of dT₇ stabilizes the native state (see below). As a consequence, the population of unfolded peptide chains drops far below 1% and no R_{ex} contributions from global folding are detectable. The remaining R_{ex} contributions in *Bs-CspB*/dT₇ originate from local unfolding mainly located in the loop regions. These loops remain dynamic on a millisecond-to-microsecond timescale even in the protein/oligonucleotide complex.

H/D exchange of amide protons in *Bs-CspB*/dT₇

Amide proton exchange is a sensitive measure for the global and local stability of a protein (63). Protons with the highest protection factors P are indicative of global unfolding, whereas protons with lower P additionally exchange by local breathing. The Gibbs free energy of unfolding of *Bs-CspB* is 12 kJ/mol, which is evident by the small protection factors of the amide protons (hatched bars in Figure 2). Most amides had fully exchanged before the first 2D ¹H-¹⁵N HSQC could be recorded after dissolving protonated ¹⁵N protein in D₂O. *Bs-CspB*/dT₇ revealed increased protection factors of amide protons in β -strands up to 10⁵. Even amides in loop β 3– β 4 are well protected. Missing bars in Figure 2 represent amides with protection factors still too small to be detected with the performed experimental setup.

DISCUSSION

Only one NMR-based complex structure of a nucleoprotein from the OB-fold family has been reported (31,32). The presented NMR structure and dynamics of *Bs-CspB* in complex with dT₇ provides now important insights into the molecular grounds of complex formation for the first representative of the CSP family. Based on the NMR data, pinpointed biochemical experiments were performed to understand the recognition of ssDNA by CSP in solution. Although CSP are believed to function *in vivo* by interaction

Table 3. Dissociation constants as well as association and dissociation rate constants of wild-type *Bs*-CspB (WT) and *Bs*-CspB variants with dT₇ and wild-type *Bs*-CspB with dT₇ derived ssDNA fragments^{a,b}

Protein + ssDNA	$K_D \times 10^{-9}$ (M)	$k_{on} \times 10^8$ (M ⁻¹ s ⁻¹)	k_{off} (s ⁻¹) ^c	k_{off} (s ⁻¹) ^d
WT <i>Bs</i> -CspB + dT ₇	1.8 ± 0.4	3.37 ± 0.11	1.7 ± 0.6	0.6 ± 0.6
K7A + dT ₇	6.4 ± 0.6	3.03 ± 0.01	5.3 ± 2.0	1.9 ± 0.2
K13Q + dT ₇	25.0 ± 3	1.45 ± 0.03	5.5 ± 0.2	3.6 ± 0.5
F15A + dT ₇	135 ± 4	1.58 ± 0.08	30.0 ± 1.6	21.3 ± 1.7
F15Y + dT ₇	1.4 ± 0.4	3.44 ± 0.10	2.2 ± 0.3	0.5 ± 0.2
F17A + dT ₇	345 ± 63	n.d.	n.d.	n.d.
D25A + dT ₇	21.4 ± 0.5	n.d.	n.d.	n.d.
F27A + dT ₇	286 ± 7	2.18 ± 0.08	103 ± 2	62.3 ± 3.8
H29Q + dT ₇	104 ± 6	2.41 ± 0.01	35.1 ± 2.3	25.1 ± 1.6
F30A + dT ₇	208 ± 11	4.29 ± 0.03	177 ± 6	89.2 ± 5.3
F30W + dT ₇	1.3 ± 0.3	4.08 ± 0.06	1.0 ± 0.4	0.5 ± 0.1
G35A + dT ₇	1.1 ± 0.3	3.18 ± 0.02	1.8 ± 1.1	0.3 ± 0.4
G35P + dT ₇	118 ± 5	2.03 ± 0.04	72.5 ± 1.1	24.0 ± 1.5
F38A + dT ₇	228 ± 9	3.34 ± 0.01	137 ± 4	76.2 ± 3.2
G54A + dT ₇	1.3 ± 0.3	2.62 ± 0.07	1.3 ± 0.8	0.3 ± 0.1
G54P + dT ₇	220 ± 9	n.d.	n.d.	n.d.
R56A + dT ₇	11.8 ± 1.4	1.39 ± 0.01	10.0 ± 1.4	1.7 ± 0.2
P58A + dT ₇	1.3 ± 0.2	4.08 ± 0.06	1.0 ± 0.7	0.5 ± 0.1
Q59A + dT ₇	2.7 ± 0.4	3.43 ± 0.01	6.1 ± 0.7	0.9 ± 0.1
WT + CTTTTTC	33.7 ± 4.1	2.58 ± 0.01	25.3 ± 2.1	8.7 ± 1.0
WT + CTCTTTC	3.9 ± 0.2	2.74 ± 0.01	4.6 ± 1.1	1.1 ± 0.1
WT + CTCTCTC	10.8 ± 0.9	2.66 ± 0.01	6.5 ± 1.2	2.9 ± 0.2
WT + CTCTTCC	66.2 ± 4.8	2.20 ± 0.02	36.1 ± 2.4	14.6 ± 1.1
WT + CTCCTTC	12.5 ± 0.6	2.64 ± 0.01	13.0 ± 0.6	3.3 ± 0.2

^aW8 could not be varied, because the quench of its fluorescence emission was used for the determination of K_D , k_{on} , and k_{off} .

^b K_D values were determined according to a 1:1 stoichiometry of protein versus oligonucleotide.

^cthe dissociation rate constant k_{off} was determined from the offset of the linear fit of experimentally observed rate constant $k_{obs} = k_{on} \bar{n} [ssDNA] + k_{off}$ at various ssDNA concentrations.

^dthe dissociation rate constant k_{off} was calculated by $k_{off} = k_{on} \bar{n} K_D$.

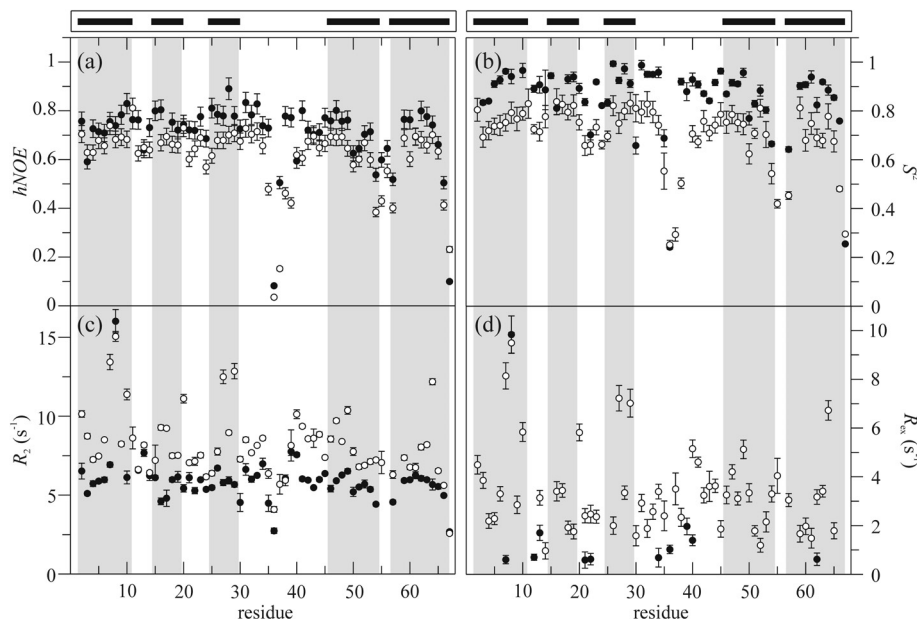


Figure 4. ¹⁵N relaxation and internal motion parameter of free (48) (open symbols) and dT₇-bound (closed symbols) *Bs*-CspB. (a) heteronuclear NOE $hNOE$ and (c) transverse relaxation rates R_2 , as well as (b) order parameters S^2 and (d) chemical exchange contributions R_{ex} to R_2 . S^2 and R_{ex} were obtained from extended Lipari-Szabo analyses of longitudinal relaxation rates R_1 (data not shown), R_2 rates and $hNOE$ using the program MODELFREE (49). Solid and gray bars represent the five β -strands of *Bs*-CspB.

with RNA, we had to choose ssDNA fragments for the current study because the quality of NMR spectra of *Bs*-CspB/RNA complexes was not sufficient for high-resolution structural investigations. A strong line broadening

of many protein resonances during titration with the RNA fragment UUAUAG reflect changes in the conformation dynamics of the complex, which require further investigations. We expect that the main findings in terms of structure

and dynamics of *Bs*-CspB in complex with ssDNA will hold for *Bs*-CspB/RNA complexes because of the following two observations. During NMR titration of *Bs*-CspB with TTATTAG (Table 1) and UUAUUAG, the chemical shifts of the same residues were affected by the nucleic acids as with dT₇ (64). The K_D of *Bs*-CspB in complex with UUAUUAG was increased by a factor of 3 compared to TTATTAG but remained in the sub-micromolar range indicating a high affinity for the RNA fragment.

Preferential binding of thymine rich ssDNA by *Bs*-CspB

Seventeen oligonucleotides were tested to identify an ssDNA fragment with high binding affinity at 1:1 stoichiometry. Table 1 confirms the earlier proposed assumption that *Bs*-CspB covers 6–7 nt with a preference for thymine rich stretches (7). Starting from dT₄, an additional thymidine decreases the K_D by a factor of 3 until the seventh thymidine, which causes a drop by a factor of 200. Above 12 and 25 nt, the stoichiometry increases from 1:1 to 2:1 and 3:1, respectively. Several fragments were derived from the putative binding site of CSP to the 5'-UTR region of the *Bs*-CspB mRNA (*cold box1* and *cold box2*) (15,65). These fragments show the general trend described above indicating that at least under *in vitro* conditions neither a preferential binding towards the cold box nor to the sense or anti-sense sequence stands out. The Y-box25 fragment had been earlier investigated with limited conclusions due to the low binding affinity, a 3:1 stoichiometry and poor NMR spectra (27). Shorter Y-box25 derived fragments showed low binding affinity.

Bs-CspB and all variants showed a strong quench of the intrinsic fluorescence, indicating that W8 is close to the binding site or at least changes the conformation of the indole ring upon binding. This is confirmed by the NMR structure and the NMR titration data, where $\Delta(\delta_{MW}^{(1H, 15N)})$ of the W8 side chain shows one of the highest values whereas the backbone is almost not affected (Figure 1). Wild-type *Bs*-CspB revealed a low preference for thymidine compared to cytidine at positions 1, 3, 4, 5 and 7 of the heptaoligomere and a moderate preference at position 6.

Independent from the analyzed protein variant and ssDNA fragment (Table 3) the association rate constant varied only marginally between $1.39 \times 10^8 \text{ M}^{-1} \text{ s}^{-1}$ and $4.29 \times 10^8 \text{ M}^{-1} \text{ s}^{-1}$. In contrast, k_{off} covered a wide range between 1.0 and 177 s^{-1} revealing a good correlation between the variation of k_{off} derived from stopped-flow experiments and the K_D values determined at equilibrium. Therefore, we propose from this extended dataset that *Bs*-CspB associates with single-stranded nucleic acids at a constant rate with a low sequence specificity. This might be important for functioning as an 'RNA chaperone' or for mapping the nucleic acid for a high affinity binding site. A low affinity of *Bs*-CspB because of a missing interaction with an essential side chain at the protein-binding site or because of a less favorable base composition at the nucleic acid is only reflected in an increased k_{off} .

Structural elucidations of *Bs*-CspB/dT₇

The structural consequences of the tight binding of *Bs*-CspB in solution have been investigated by NMR spectroscopy. To localize the binding site for dT₇ we employed both the change in protein chemical shifts during NMR titration experiments (blue in Figure 5) and the mutational data (yellow in Figure 5). Differences in the backbone conformation between free and complexed *Bs*-CspB are mainly located in the loops $\beta 1$ – $\beta 2$ and $\beta 3$ – $\beta 4$. These stretches correspond to the group of residues with high $\Delta(\delta_{MW}^{(1H, 15N)})$ values including the proposed RNP1 (13–20) and RNP2 (26–30) motives (28,29). The mutational data revealed the importance of the side chains of F15, F17, F27, H29, F30 and F38 (yellow in Figure 5). All these residues showed also high $\Delta(\delta_{MW})$ values of the backbone resonances. Additionally, the side chains of W8, F15, D25, F30, Q34, Q59 and N62 stand out from changes in chemical shifts upon binding. For the here reported representative of CSP, the tertiary structure of the five β -strands are almost invariant upon binding. From those OB-fold proteins, where the structure of both the free and nucleic acid-bound state are known, large conformational changes were mainly reported for loop $\beta 1$ – $\beta 2$ and for the relative orientation of several mainly invariant OB-fold domains

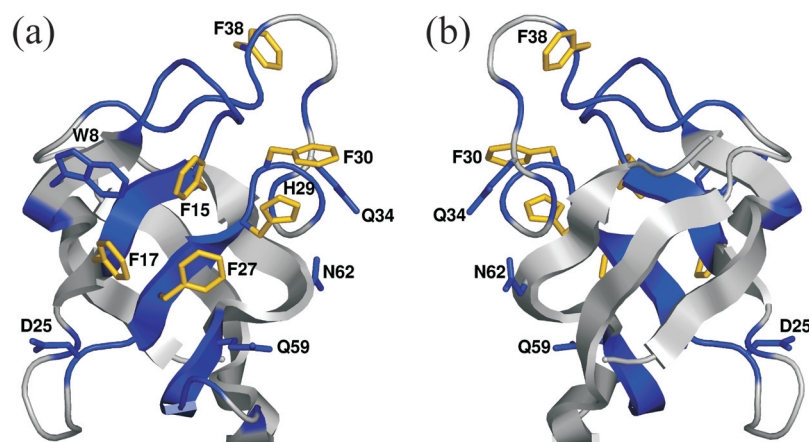


Figure 5. Nucleic acid-binding site of *Bs*-CspB determined by NMR spectroscopy and site-directed mutagenesis at (a) front view and (b) back view. The following residues experienced substantial chemical shift changes of their NMR resonances upon binding to dT₇ and are indicated in blue: 7, 10–17, 20, 25, 26–31, 33, 35, 38–42, 54, 56–59 (backbone) and 8, 25, 34, 59, 62 (side chain). Yellow highlighted side chains illustrate aromatic residues, for which the K_D increased above 100 nM after substitution with alanine. For this illustration the NMR structure with the lowest energy was used.

recognizing larger stretches of ssDNA or ssRNA (30). We can conclude that CSP also use the β -barrel as scaffold for ssDNA recognition, which is a general feature of OB-fold proteins, and loop β 3– β 4 to extend the ssDNA recognition site. With only 67 residues, *Bs*-CspB is one of the smallest OB-fold proteins.

These structural elucidations in solution of the *Bs*-CspB conformation and ssDNA-binding site in *Bs*-CspB/dT₇ are in very good agreement with the structure of *Bs*-CspB/dT₆ determined by X-ray crystallography (2ES2.pdb; Max *et al.*, manuscript to be published elsewhere). All residues, which are in contact with the ssDNA via the backbone showed high $\Delta(\delta_{\text{MW}})$ values of the amides and/or the H $^{\alpha}$ /C $^{\alpha}$ nuclei. All residues with side chains involved in stacking interactions or hydrogen bonds stand out as well from the $\Delta(\delta_{\text{MW}})$ and $\Delta(\delta(^1\text{H}))$ values. The superposition of the 18 lowest energy NMR structures and the crystal structure is given in Figure 6. It revealed an averaged root mean square deviation (r.m.s.d.) for the heavy backbone atoms of residues 1–67 of 1.44 Å (Table 2). Remaining deviations are located in the loops β 2– β 3, β 3– β 4 and β 4– β 5. It is unlikely that binding of the ssDNA causes the deviation of loop β 2– β 3 because the C-terminal part of loop β 2– β 3 (Q21–D25) depicts the same deviation between NMR structure and X-ray structure for the free form and between X-ray structures of *Bs*-CspB determined at different resolutions (1CSP.pdb and 1CSQ.pdb). For a comparison of the side chain conformations between solution and the crystal structure we have to consider on the NMR side the missing dT₇ moiety. Still, W8 is well defined and adopts in solution a conformation different from the crystal structure and the free protein. F38 in loop β 3– β 4 is involved in dT₇ binding shown by the increased K_{D} of the F38A variant, the increase of the backbone S^2 indicating a reduction in dynamics and the exchange protected amide proton of adjacent G37 in *Bs*-CspB/dT₇. Beside W8 and F38, all aromatic side chains involved in dT₇ stacking form in solution a very similar ssDNA recognition pattern compared to the crystal.

Dynamics and stability of *Bs*-CspB/dT₇

Binding of nucleic acids changes the dynamics and stability of the interacting protein. For an induced fit mechanism one would expect a dynamic recognition site (66). A reduction in the sub-nanosecond dynamics upon binding has been reported, for example, for the DNA-binding loop of the Lac-repressor head piece, which forms a rigid hinge helix upon binding to cognate DNA operators (67). Additionally, the protection factors of the amide protons of this protein increased globally after complex formation by five orders of magnitude (68). Therefore, a change in the relaxation and H/D exchange rates upon binding and a comparison of the derived order parameters, chemical exchange rates and protection factors with the values of the free protein are additional indicators for ssDNA binding to sole chemical shift changes.

Correlating the backbone r.m.s.d. values of the family of presented *Bs*-CspB structures in the *Bs*-CspB/dT₇ complex with general order parameters S^2 reveal those regions, which do not converge during structure calculation due to sub-nanosecond dynamics. Residues 34–41 in loop β 3– β 4 exhibit increased internal dynamics in the free protein (Figure 4) but

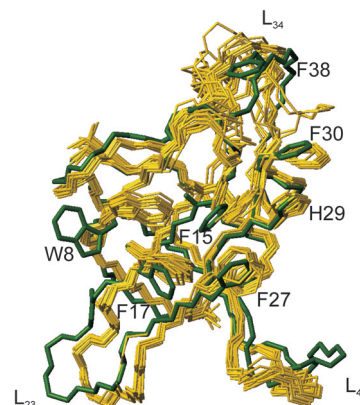
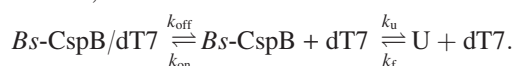


Figure 6. Backbone superposition of the 18 lowest energy NMR structures (yellow) of *Bs*-CspB/dT₇ and the crystal structure (green) of *Bs*-CspB/dT₆ (2ES2.pdb). The side chain conformations of the aromatic residues, which facilitate binding of dT₇, are depicted and labeled.

only G35, E36 and G37 remain dynamic in the *Bs*-CspB/dT₇ complex indicating that binding of dT₇ reduces the local dynamics of the C-terminal end of loop β 3– β 4. All side chains involved in ssDNA binding are presented by free *Bs*-CspB on a backbone, which is rigid on the sub-nanosecond timescale.

Bs-CspB functions as a CSP implying a strong temperature dependence of the nucleic acid affinity. Indeed, we found a strong increase of K_{D} with increasing temperature of *Bs*-CspB/dT₇: 1.8 ± 0.4 nM at 15°C, 60 ± 4 nM at 25°C and 464 ± 31 nM at 35°C. This suggests a strong entropic contribution counterbalancing the gain in Gibbs free energy upon ssDNA binding. Thermodynamic contributions from the folding–unfolding equilibrium of CspB in this temperature range are expected to be small because binding and stability of CspB are not correlated (27) and the increase of the population of the unfolded state of free CspB between 15 and 35°C is below 5% (69). From the reduction of backbone dynamics in *Bs*-CspB/dT₇, revealed by comparing S^2 values of free and bound *Bs*-CspB, the contribution to the entropy change of the protein chain upon binding can be estimated on a nanosecond-to-picosecond timescale (70,71). The sum of this conformational entropy change associated with the individual N-H bond vectors results in -470 J/(mol·K).

Two further observations by NMR spectroscopy show that dT₇ stabilizes *Bs*-CspB globally during complex formation: a significant reduction of chemical exchange rate constants R_{ex} (Figure 4) and an increase of protection of amide protons against exchange (Figure 2). We attribute the change in R_{ex} to a shift of the equilibrium between folded and unfolded *Bs*-CspB towards the native, dT₇ bound state. At 0.7 mM *Bs*-CspB, the pseudo first-order association rate constant exceeds $200\,000$ s⁻¹ and the population of uncomplexed *Bs*-CspB at a K_{D} of 1.8 nM is too small to give rise to R_{ex} contributions from the binding reaction or the folding–unfolding reaction of free *Bs*-CspB assuming the following simple scheme, where U denotes the unfolded state of *Bs*-CspB:



A loss in detectable R_{ex} contributions to the transverse relaxation rate because of a stabilization of *Bs*-CspB by

ethylene glycol has been reported previously and discussed (48,62). For the most protected amide protons, only the global unfolding of the entire polypeptide chain will allow exchange with deuterium and the rate of exchange must be much slower than the folding rate to derive thermodynamic stability data from H/D exchange rates (EX2 limit). This has been confirmed for free *Bs*-CspB by the pH dependence of the exchange rate between pH 6 and 7 (data not shown). A K_D in the nM range increases the protection factor by several orders of magnitude, if only the unfolded state U is the exchange competent form, which has been observed for example for the Lac-repressor headpiece during binding with DNA operators (68). For *Bs*-CspB, the equivalent global effect was detected (Figure 2). However, the protection factors increased only by a factor of 1000, which is about two orders of magnitude lower than expected for the simple three-state model depicted above. Therefore, we assume that despite the low dissociation constant, the *Bs*-CspB/dT₇ complex remains dynamic so that there is still enough local unfolding present to explain the observed H/D exchange rates.

ACKNOWLEDGEMENTS

We thank P. Rösch, H. Kessler and P. E. Wright for NMR spectrometer time at 600, 750 and 900 MHz, respectively, F. X. Schmid for very helpful discussions, and T. Haslberger for the study with UUAUUAG. This research was supported by grants from the Fonds der Chemischen Industrie (FCI) and the Deutsche Forschungsgemeinschaft (Ba 1821/3-1,2 and SFB473). Funding to pay the Open Access publication charges for this article was provided by FCI and the state network of excellence (Sachsen-Anhalt).

Conflict of interest statement. None declared.

REFERENCES

- Graumann,P.L. and Marahiel,M.A. (1998) A superfamily of proteins that contain the cold-shock domain. *Trends Biochem. Sci.*, **23**, 286–290.
- Jones,P.G., van Bogelen,R.A. and Neidhardt,F.C. (1987) Induction of proteins in response to low temperature in *Escherichia coli*. *J. Bacteriol.*, **169**, 2092–2095.
- Jones,P.G. and Inouye,M. (1996) RbfA, a 30S ribosomal binding factor, is a cold-shock protein whose absence triggers the cold-shock response. *Mol. Microbiol.*, **21**, 1207–1218.
- Phadtare,S., Inouye,M. and Severinov,K. (2002) The nucleic acid melting activity of *Escherichia coli* CspE is critical for transcription antitermination and cold acclimation of cells. *J. Biol. Chem.*, **277**, 7239–7245.
- Jones,P.G., Krah,R., Tafuri,S.R. and Wolffe,A.P. (1992) DNA gyrase, CS7.4, and the cold shock response in *Escherichia coli*. *J. Bacteriol.*, **174**, 5798–5802.
- Jiang,W., Hou,Y. and Inouye,M. (1997) CspA, the major cold-shock protein of *Escherichia coli*, is an RNA chaperone. *J. Biol. Chem.*, **272**, 196–202.
- Lopez,M.M., Yutani,K. and Makhatadze,G.I. (1999) Interactions of the major cold shock protein of *Bacillus subtilis* CspB with single-stranded DNA templates of different base composition. *J. Biol. Chem.*, **274**, 33601–33608.
- Lopez,M.M. and Makhatadze,G.I. (2000) Major cold shock proteins, CspA from *Escherichia coli* and CspB from *Bacillus subtilis*, interact differently with single-stranded DNA templates. *Biochim. Biophys. Acta*, **1479**, 196–202.
- Lopez,M.M., Yutani,K. and Makhatadze,G.I. (2001) Interactions of the cold shock protein CspB from *Bacillus subtilis* with single-stranded DNA. Importance of the T base content and position within the template. *J. Biol. Chem.*, **276**, 15511–15518.
- Bae,W., Xia,B., Inouye,M. and Severinov,K. (2000) *Escherichia coli* CspA-family RNA chaperones are transcription antiterminators. *Proc. Natl Acad. Sci. USA*, **97**, 7784–7789.
- Phadtare,S., Tyagi,S., Inouye,M. and Severinov,K. (2002) Three amino acids in *Escherichia coli* CspE surface-exposed aromatic patch are critical for nucleic acid melting activity leading to transcription antitermination and cold acclimation of cells. *J. Biol. Chem.*, **277**, 46706–467011.
- Stulke,J. (2002) Control of transcription termination in bacteria by RNA-binding proteins that modulate RNA structures. *Arch. Microbiol.*, **177**, 433–440.
- Hofweber,R., Horn,G., Langmann,T., Balbach,J., Kremer,W., Schmitz,G. and Kalbitzer,H.R. (2005) The influence of cold shock proteins on transcription and translation studied in cell-free model systems. *FEBS J.*, **272**, 4691–4702.
- Xia,B., Etchegaray,J.P. and Inouye,M. (2001) Nonsense mutations in *cspA* cause ribosome trapping leading to complete growth inhibition and cell death at low temperature in *Escherichia coli*. *J. Biol. Chem.*, **276**, 35581–35588.
- Xia,B., Ke,H., Jiang,W. and Inouye,M. (2002) The Cold Box stem-loop proximal to the 5'-end of the *Escherichia coli cspA* gene stabilizes its mRNA at low temperature. *J. Biol. Chem.*, **277**, 6005–6011.
- Yamanaka,K., Fang,L. and Inouye,M. (1998) The CspA family in *Escherichia coli*: multiple gene duplication for stress adaptation. *Mol. Microbiol.*, **27**, 247–255.
- Graumann,P., Wendrich,T.M., Weber,M.H., Schröder,K. and Marahiel,M.A. (1997) A family of cold shock proteins in *Bacillus subtilis* is essential for cellular growth and for efficient protein synthesis at optimal and low temperatures. *Mol. Microbiol.*, **25**, 741–756.
- Murzin,A.G. (1993) OB(oligonucleotide/oligosaccharide binding)-fold: common structural and functional solution for non-homologous sequences. *EMBO J.*, **12**, 861–867.
- Schnuchel,A., Wiltschek,R., Czisch,M., Herrler,M., Willimsky,G., Graumann,P., Marahiel,M.A. and Holak,T.A. (1993) Structure in solution of the major cold-shock protein from *Bacillus subtilis*. *Nature*, **364**, 169–171.
- Schindelin,H., Marahiel,M.A. and Heinemann,U. (1993) Universal nucleic acid-binding domain revealed by crystal structure of the *B. subtilis* major cold-shock protein. *Nature*, **364**, 164–168.
- Feng,W., Tejero,R., Zimmerman,D.E., Inouye,M. and Montelione,G.T. (1998) Solution NMR structure and backbone dynamics of the major cold-shock protein (CspA) from *Escherichia coli*: evidence for conformational dynamics in the single-stranded RNA-binding site. *Biochemistry*, **37**, 10881–10896.
- Newkirk,K., Feng,W., Jiang,W., Tejero,R., Emerson,S.D., Inouye,M. and Montelione,G.T. (1994) Solution NMR structure of the major cold shock protein (CspA) from *Escherichia coli*: identification of a binding epitope for DNA. *Proc. Natl Acad. Sci. USA*, **91**, 5114–5118.
- Schindelin,H., Jiang,W.N., Inouye,M. and Heinemann,U. (1994) Crystal structure of CspA, the major cold shock protein of *Escherichia coli*. *Proc. Natl Acad. Sci. USA*, **91**, 5119–5123.
- Mueller,U., Perl,D., Schmid,F.X. and Heinemann,U. (2000) Thermal stability and atomic-resolution crystal structure of the *Bacillus caldolyticus* cold shock protein. *J. Mol. Biol.*, **297**, 975–988.
- Kremer,W., Schuler,B., Harrieder,S., Geyer,M., Gronwald,W., Welker,C., Jaenicke,R. and Kalbitzer,H.R. (2001) Solution NMR structure of the cold-shock protein from the hyperthermophilic bacterium *Thermotoga maritima*. *Eur. J. Biochem.*, **268**, 2527–2539.
- Schindler,T., Perl,D., Graumann,P., Sieber,V., Marahiel,M.A. and Schmid,F.X. (1998) Surface-exposed phenylalanines in the RNP1/RNP2 motif stabilize the cold-shock protein CspB from *Bacillus subtilis*. *Proteins*, **30**, 401–406.
- Zeeb,M. and Balbach,J. (2003) Single-stranded DNA binding of the cold shock protein CspB from *Bacillus subtilis*: NMR mapping and mutational characterisation. *Protein Sci.*, **12**, 112–123.
- Schröder,K., Graumann,P., Schnuchel,A., Holak,T.A. and Marahiel,M.A. (1995) Mutational analysis of the putative nucleic acid-binding surface of the cold-shock domain, CspB, revealed an essential role of aromatic and basic residues in binding of single-stranded DNA containing the Y-box motif. *Mol. Microbiol.*, **16**, 699–708.

29. Graumann,P. and Marahiel,M.A. (1996) A case of convergent evolution of nucleic acid binding modules. *Bioessays*, **18**, 309–315.
30. Theobald,D.L., Mitton-Fry,R.M. and Wuttke,D.S. (2003) Nucleic acid recognition by OB-fold proteins. *Annu. Rev. Biophys. Biomol. Struct.*, **32**, 115–133.
31. Mitton-Fry,R.M., Anderson,E.M., Hughes,T.R., Lundblad,V. and Wuttke,D.S. (2002) Conserved structure for single-stranded telomeric DNA recognition. *Science*, **296**, 145–147.
32. Mitton-Fry,R.M., Anderson,E.M., Theobald,D.L., Glustrom,L.W. and Wuttke,D.S. (2004) Structural basis for telomeric single-stranded DNA recognition by yeast Cdc13. *J. Mol. Biol.*, **338**, 241–255.
33. Schindler,T., Herrler,M., Marahiel,M.A. and Schmid,F.X. (1995) Extremely rapid folding in the absence of intermediates: the cold-shock protein from *Bacillus subtilis*. *Nature Struct. Biol.*, **2**, 663–673.
34. Grzesiek,S., Stahl,S.J., Wingfield,P.T. and Bax,A. (1996) The CD4 determinant for downregulation by HIV-1 Nef directly binds to Nef. Mapping of the Nef binding surface by NMR. *Biochemistry*, **35**, 10256–10261.
35. Wittekind,M. and Mueller,L. (1993) HNCACB, a high-sensitivity 3D NMR experiment to correlate amideproton and nitrogen resonances with the alpha- and beta-carbon resonances in proteins. *J. Magn. Reson.*, **101**, 201–205.
36. Grzesiek,S. and Bax,A. (1992) Correlating backbone amide and side chain resonances in larger proteins by multiple relayed triple resonance NMR. *J. Am. Chem. Soc.*, **114**, 6291–6293.
37. Grzesiek,S., Anglister,J. and Bax,A. (1993) Correlation of backbone amide and aliphatic sidechain resonances in $^{13}\text{C}/^{15}\text{N}$ -enriched proteins by isotropic mixing of ^{13}C magnetization. *J. Magn. Reson. B*, **101**, 114–119.
38. Bax,A., Clore,G.M. and Gronenborn,A.M. (1990) ^1H - ^1H correlation via isotropic mixing of ^{13}C magnetization, a new three-dimensional approach for assigning ^1H and ^{13}C spectra of ^{13}C -enriched proteins. *J. Magn. Reson.*, **88**, 425–431.
39. Yamazaki,T., Forman-Kay,J.D. and Kay,L.E. (1993) Two-dimensional NMR experiments for correlating ^{13}C and ^1H / chemical shifts of aromatic residues in ^{13}C -labeled proteins via scalar couplings. *J. Am. Chem. Soc.*, **115**, 11054–11055.
40. Talluri,S. and Wagner,G. (1996) An optimized 3D NOESY-HSQC. *J. Magn. Res.*, **112B**, 200–205.
41. Otting,G. and Wüthrich,K. (1989) Extended heteronuclear editing of 2D 1H NMR spectra of isotope-labeled proteins, using $x(w1,w2)$ double half filter. *J. Magn. Reson.*, **85**, 586–594.
42. Zwahlen,C., Legault,P., Vincent,S.J.F., Greenblatt,J., Konrat,R. and Kay,L.E. (1997) Methods for measurement of intermolecular NOEs by multinuclear NMR spectroscopy: application to a bacteriophage α N-peptide/boxB RNA complex. *J. Am. Chem. Soc.*, **119**, 6711–6721.
43. Sattler,M., Schleucher,J. and Griesinger,C. (1999) Heteronuclear multidimensional NMR experiments for the structure determination of proteins in solution employing pulsed field gradients. *Prog. NMR Spectrosc.*, **34**, 93–158.
44. Vuister,G.W. and Bax,A. (1993) Quantitative J correlation: a new approach for measuring homonuclear three-bond J(HNHa) coupling constants in ^{15}N -enriched proteins. *J. Am. Chem. Soc.*, **115**, 7772–7777.
45. Hansen,M.R., Mueller,L. and Pardi,A. (1998) Tunable alignment of macromolecules by filamentous phage yields dipolar coupling interactions. *Nature Struct. Biol.*, **5**, 1065–1074.
46. Gibbs,S.J. and Johnson,C.S., Jr. (1991) A PFG NMR experiment for accurate diffusion and flow studies in the presence of eddy currents. *J. Magn. Reson.*, **93**, 395–402.
47. Bai,Y.W., Milne,J.S., Mayne,L. and Englander,S.W. (1994) Protein stability parameters measured by hydrogen exchange. *Proteins*, **20**, 4–14.
48. Zeeb,M., Jacob,M.H., Schindler,T. and Balbach,J. (2003) ^{15}N relaxation study of the cold shock protein CspB at various solvent viscosities. *J. Biomol. NMR*, **27**, 221–234.
49. Palmer,A.G., III, Rance,M. and Wright,P.E. (1991) Intramolecular motions of a zinc finger DNA-binding domain from xfin characterized by proton detected natural abundance C-13 heteronuclear NMR spectroscopy. *J. Am. Chem. Soc.*, **113**, 4371–4380.
50. Karplus,M. (1959) Contact electron-spin coupling of nuclear magnetic moments. *J. Chem. Phys.*, **30**, 11–15.
51. Schwieters,C.D., Kuszewski,J.J., Tjandra,N. and Clore,G.M. (2003) The Xplor-NIH NMR molecular structure determination package. *J. Magn. Reson.*, **160**, 65–73.
52. Nilges,M. (1998) Ambiguous NOEs and automated NOE assignment. *Prog. NMR spectrosc.*, **32**, 107.
53. Folmer,R.H., Hilbers,C.W., Konings,R.N. and Nilges,M. (1997) Floating stereospecific assignment revisited: application to an 18 kDa protein and comparison with J-coupling data. *J. Biomol. NMR*, **9**, 245–258.
54. Kuszewski,J. and Clore,G.M. (2000) Sources of and solutions to problems in the refinement of protein NMR structures against torsion angle potentials of mean force. *J. Magn. Reson.*, **146**, 249–254.
55. Neudecker,P., Sticht,H. and Rosch,P. (2001) Improving the efficiency of the Gaussian conformational database potential for the refinement of protein and nucleic acid structures. *J. Biomol. NMR*, **21**, 373–375.
56. Schweimer,K., Hoffmann,S., Bauer,F., Friedrich,U., Kardinal,C., Feller,S.M., Biesinger,B. and Sticht,H. (2002) Structural investigation of the binding of a herpesviral protein to the SH3 domain of tyrosine kinase Lck. *Biochemistry*, **41**, 5120–5130.
57. Kabsch,W. and Sander,C. (1983) Dictionary of protein secondary structure: pattern recognition of hydrogen-bonded and geometrical features. *Biopolymers*, **22**, 2577–2637.
58. Wallace,A.C., Laskowski,R.A. and Thornton,J.M. (1996) Derivation of 3D coordinate templates for searching structural databases: application to Ser-His-Asp catalytic triads in the serine proteinases and lipases. *Protein Sci.*, **5**, 1001–1013.
59. Laskowski,R.A., Rullmann,J.A., MacArthur,M.W., Kaptein,R. and Thornton,J.M. (1996) AQUA and PROCHECK-NMR: programs for checking the quality of protein structures solved by NMR. *J. Biomol. NMR*, **8**, 477–486.
60. Koradi,R., Billeter,M. and Wüthrich,K. (1996) MOLMOL: a program for display and analysis of macromolecular structures. *J. Mol. Graph.*, **14**, 51–55.
61. Zeeb,M. and Balbach,J. (2005) Millisecond protein folding studied by NMR spectroscopy. *Protein Pept. Lett.*, **12**, 139–146.
62. Zeeb,M. and Balbach,J. (2005) NMR spectroscopic characterization of millisecond protein folding by transverse relaxation dispersion measurements. *J. Am. Chem. Soc.*, **127**, 13207–13012.
63. Englander,S.W., Sosnick,T.R., Englander,J.J. and Mayne,L. (1996) Mechanisms and uses of hydrogen exchange. *Curr. Opin. Struct. Biol.*, **6**, 18–23.
64. Haslberger,T. (2004) Spectroscopic investigations of the function and folding of the cold shock protein B from *Bacillus subtilis*. Diploma thesis, University of Bayreuth.
65. Fang,L., Hou,Y. and Inouye,M. (1998) Role of the cold-box region in the 5' untranslated region of the cspA mRNA in its transient expression at low temperature in *Escherichia coli*. *J. Bacteriol.*, **180**, 90–95.
66. Carr,P.A., Erickson,H.P. and Palmer,A.G., III (1997) Backbone dynamics of homologous fibronectin type III cell adhesion domains from fibronectin and tenascin. *Structure*, **5**, 949–959.
67. Slijper,M., Boelens,R., Davis,A.L., Konings,R.N., van der Marel,G.A., van Boom,J.H. and Kaptein,R. (1997) Backbone and side chain dynamics of lac repressor headpiece (1–56) and its complex with DNA. *Biochemistry*, **36**, 249–254.
68. Kalodimos,C.G., Boelens,R. and Kaptein,R. (2002) A residue-specific view of the association and dissociation pathway in protein–DNA recognition. *Nature Struct. Biol.*, **9**, 193–197.
69. Perl,D., Mueller,U., Heinemann,U. and Schmid,F.X. (2000) Two exposed amino acid residues confer thermostability on a cold shock protein. *Nature Struct. Biol.*, **7**, 380–383.
70. Yang,D. and Kay,L.E. (1996) Contributions to conformational entropy arising from bond vector fluctuations measured from NMR-derived order parameters: application to protein folding. *J. Mol. Biol.*, **263**, 369–382.
71. Yang,D., Mok,Y.K., Forman-Kay,J.D., Farrow,N.A. and Kay,L.E. (1997) Contributions to protein entropy and heat capacity from bond vector motions measured by NMR spin relaxation. *J. Mol. Biol.*, **272**, 790–804.